Geochemistry of the unusual mafic intrusions in Betul Fold Belt, Central India: implications for Ni–Cu–Au–PGE metallogeny

D. V. Subba Rao[1,*], M. Satyanarayanan[1], D. Srinivasa Sarma[1], K. S. V. Subramanyam[1], K. Venkateswarlu[1] and M. Hanuma Prasad[2]

[1]CSIR-National Geophysical Research Institute, Hyderabad 500 007, India
[2]Geomysore Services (India) Pvt Ltd, Bengaluru 560 037, India

We report here the recent occurrence of native gold and platinoids, associated with Fe–Ni–Cu–Pb–Zn sulphides and tungsten-bearing phases in the gabbroic intrusions emplaced in the Betul–Chhindwara Belt in the Central Indian Tectonic Zone (CITZ). The ore minerals are represented mainly by native gold, pentlandite, chalcopyrite, pyrite, bowieite and rare phases of tungsten, cadmium and palladium, which were identified by scanning electron microscopy. The whole rock geochemistry shows anomalous Ni–Cu and platinum group elements (PGE) in which palladium is always higher in concentration than in platinum. The inter-element relationships of PGE such as Pd versus Ir and Pt versus Ir indicate their fractionation by a sulphide phase and also suggest that the parental magmas are primitive in nature having high-Mg, low-Ti characteristics, which indicate the boninitic/picritic nature of magmas. A thorough investigation is essential for exploring the Betul mafic–ultramafic intrusions for proving their potential as the host rocks for Au and Ni–Cu–PGE ores.

Keywords: Gabbro intrusions, geochemistry, CITZ, native gold, platinum group elements,

GABBROIC intrusions occur in a variety of tectonic environments such as the older greenstone belts in Zimbabwe, Kaapvaal, South Africa; Yilgarn, Australia; Dharwar Craton, India and Jinchuan, China[1] as well as the Tertiary intrusions which are associated with continental rifting such as those at Skaergaard, East Greenland and Rhum, Australia. These intrusions are of great economic significance as they host virtually all the known world resources of PGE, chromite as well as important ore deposits of V, Ti, Cu and Ni. Majority of such magmatic Ni–Cu–PGE deposits are associated with mantle-derived mafic–ultramafic complexes. Similar geological settings and lithological associations occur in India which await detailed assessment for Ni–Cu–PGE mineralization. The Betul ultramafic–mafic complex forms an integral part of Central Indian Tectonic Zone (CITZ), wherein extensive mafic–ultramafic intrusions are well-exposed. The need to assess these largely unexplored intrusions towards a better understanding of their emplacement history and differentiation processes, has prompted a systematic study of the Betul mafic intrusion from central India in terms of its tectonic setting, geochemical characteristics, nature of parental magmas and PGE geochemistry.

The Betul Fold Belt (BFB) occurs in the south-western part of CITZ, which is a composite zone (~200 km long and trending ENE–WSW) which runs across the Peninsular Shield. CITZ is aligned parallel to the Son–Narmada North Fault (SNNF) in the north and the Central Indian Suture (CIS) in the south and constitutes several Proterozoic mobile belts (Figure 1) such as Mahakoshal Belt (2.2–1.8 Ga), Betul Belt (1.8–0.85 Ga), Sausar Belt (1.1–0.95 Ga), Sakoli Belt (~2.0 Ga) and Kotri Belt[2]. These belts are interspersed by three granulite zones such as Ramakona Granulite Belt (RKG), Makrohar Granulite Belt (MGB) and the Balaghat–Bhandara Granulite Belt (BBG)[2]. Based on metamorphic and geochronological studies, several workers[2–4,8] have suggested that the Satpura Mountain Belt (also called as CITZ) represents a zone of collision between the Southern Cratonic Block (SCB) and the Northern Cratonic Block (NCB) (Figure 1 *a*). This collisional or tectono-thermal event has been correlated with the Grenville orogeny at ~1100 Ma (ref. 5), ~1000 Ma (ref. 6) and between 1000 and 900 Ma (ref. 2). The Proterozoic Betul intrusive complex in Central India forms a part of the BFB. It has a ENE–WSW strike and extends for about 150 km from Chichola to Chhindwara, having a width varying from 20 to 30 km (Figure 1 *b* and *c*). Precise radioactive U–Pb ages are not available. Two Rb–Sr ages of 1550 ± 50 and 850 ± 15 Ma[7] were obtained on the syn-tectonic intrusive granites and granitoids from Betul belt, which were interpreted as the maximum and minimum age limits for the Betul supracrustal rocks. The rocks of the belt have undergone medium-grade amphibolite facies metamorphism and three phases of deformation. The extensive plutonic suite of mafic–ultramafic rocks in the NW part of the Betul complex occurring at Temra area as well as at the Sarni area in the SE part of the belt are investigated in this study. The Temra and Sarni matagabbros and anorthositic gabbros show extensive sulphide alteration haloes/gossans and are intruded by pink quartz veins with visible sulphide-bearing zones. Metagabbros are associated with metapyroxenites which form differentiated large ultramafic–mafic intrusions. Extensive sulphide mineralization within meta gabbro suite at Temra site have earlier been identified during their preliminary surveys by M/s Geomysore Services (India) Pvt Ltd, Bangalore as well as the Geological Survey of India (GSI Portal; FSP Code 2010791). In contrast, volcanic hosted massive sulphide deposits (VMS type) within the felsic volcanic horizons of Betul Belt were also identified by earlier workers which show hydrothermal alterations associated with base metal sulphides formed due to submarine volcanic

*For correspondence. (e-mail: dvsubbarao3s@rediffmail.com)

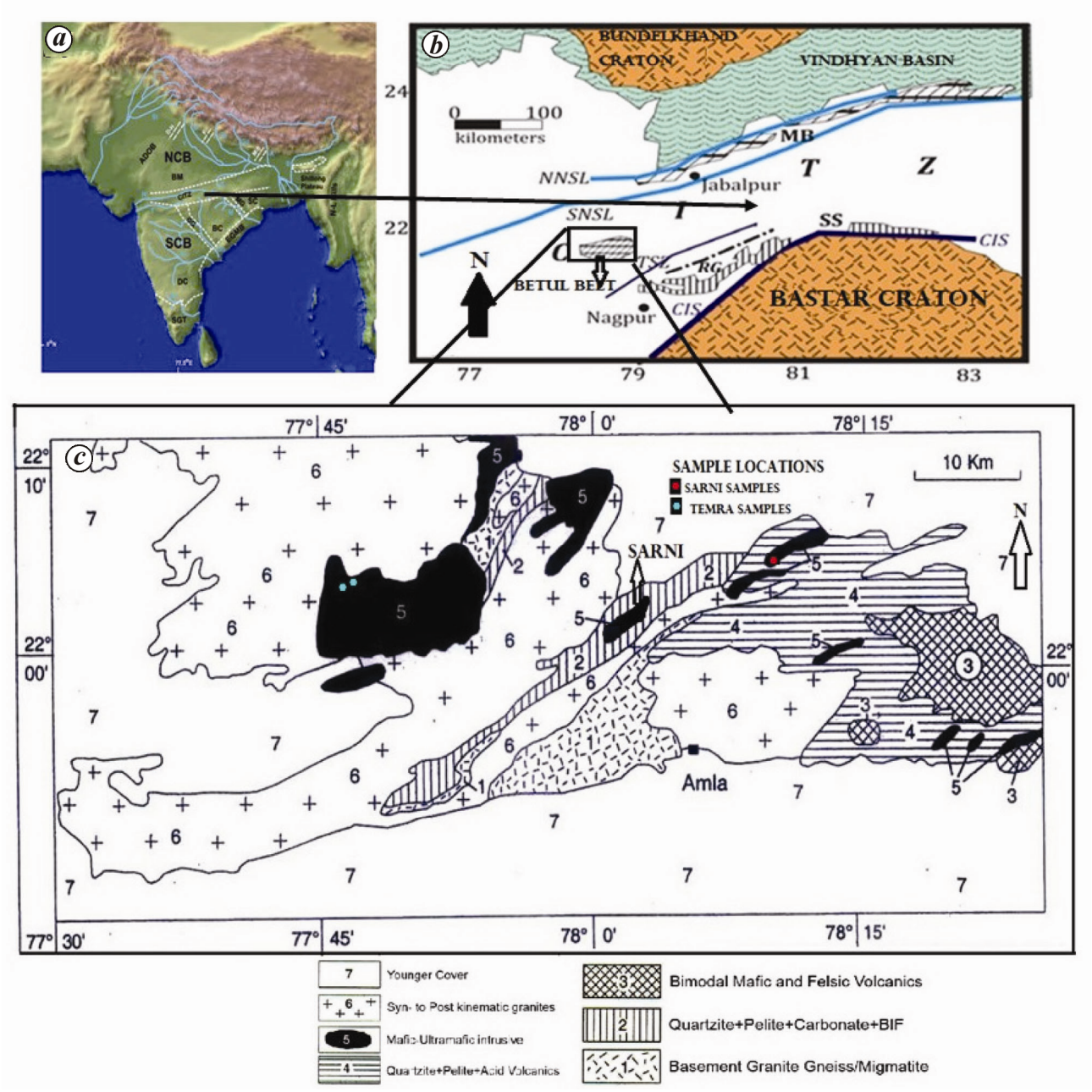

Figure 1. ***a***, Map of India showing its crustal architecture, CITZ = Central Indian tectonic zone, which separates the two cratonic blocks such as the northern cratonic block (NCB) and larger southern cratonic block (map after Deb[18]). ***b***, Generalized geological map of Betul Belt (map after Acharya[19] and Meert *et al.*[20]). ***c***, Geological map of Betul Belt showing the location of the samples studied and predominance of mafic–ultramafic intrusions in the Betul Belt (Roy *et al.*[21]).

activity[9–11]. The Temra metagabbro/anorthositic gabbro suite located at 22°06′35.3″N and 77°46′50.0″E, is massive, medium-grained, melanocratic, consists of plagioclase, relict clinopyroxenes and a variety of amphiboles as essential minerals, whereas titanite, opaques and other sulphides are accessory phases. The twinned plagioclases of Temra anorthositic gabbros show cumulus textures with interstitial mafic minerals. Triple junctions are also observed between the laths of plagioclase grown up to 1 mm in size. Plagioclases also display micro-deformation structures such as grain boundary granulation, distorted and bent twin lamellae. Opaque minerals show replacement textures evidenced by remnants of host silicates occurring as inclusions. The metagabbros exhibit granular, ophitic to subophitic textures where the primary magmatic amphiboles observed are of tremolite, magnesio-hornblende and actinolite compositions. At places, sericitization of plagioclase along the grain margins is observed. Titanite shows thin exsolution lamellae of opaques along the cleavage planes. The Sarni metagabbros

in this study located at 22°04′46.3″N and 78°9′34.8″E have plagioclase, amphiboles and relict clinopyroxenes as essential minerals, whereas opaques and titanites form the accessory mineral phases. When compared to the metagabbros of Temra, the pyroxenes, amphiboles and plagioclases of Sarni are highly altered. This is evidenced by the presence of resorbed plagioclase grain boundaries, relict clinopyroxenes and skeletal remains of amphiboles within opaques. Chemical compositions of the coexisting silicate minerals were determined by CAMECA-SX-100 electron microprobe at CSIR-NGRI. Carbon-coated polished thin sections were used for electron probe micro analysis. Major elements standards supplied by Cameca were used for major element calibration. Si, Ca and Fe were calibrated using andradite, Na on Jadeite, Al on Corundum, K on orthoclase and Ti, Cr, Mn, Mg using standards of respective elements. An electron beam was produced by a tungsten filament of 1–3 μm with 20 kV accelerating voltage having 20 nA beam current at 10^{-6} Pa vacuum. The element concentrations are measured on a Faraday cup detector. Peak and background counting times were 50 sec and 25 sec respectively. Repeated analysis of standards during the analytical sessions spread over several days suggests less than 1% analytical error in the data obtained. The analytical data is summarized in Tables 1 and 2.

Feldspars are composed mainly of coarse-grained well-twinned unaltered calcic plagioclase laths with bytownite composition ($An_{73–76}Ab_{24–27}Or_{0.1–0.3}$) that show no compositional zoning (Table 1). Amphiboles are magnesiohornblende as well as actinolite in composition (X_{Mg} = 0.75–0.85) (Table 2). Opaques are represented mainly by Ni–Fe–Cu sulphides, and subordinate Cr–Fe–Ti oxides as well as discrete grains of bowieite (RhS), native gold, pyrrhotite and pentlandite occurring as disseminations. Chalcopyrite and pyrite show coarse segregations/clots, stringers within altered/sheared metagabbros. Discrete grains of pentlandite are observed. The

Table 1. Plagioclase composition data of Temra metagabbros

Point	1	2	3	4	5	6
SiO_2 (wt%)	48.72	49.62	49.53	49.32	47.96	48.54
TiO_2	0.00	0.00	0.01	0.03	0.00	0.01
Al_2O_3	32.50	32.32	32.26	30.63	31.22	29.78
Cr_2O_3	0.00	0.01	0.00	0.00	0.00	0.02
FeO	0.03	0.05	0.09	0.04	0.04	0.03
MnO	0.04	0.00	0.00	0.00	0.00	0.00
MgO	0.00	0.00	0.00	0.00	0.00	0.01
CaO	17.14	16.56	16.66	17.21	17.52	16.74
Na_2O	3.02	3.32	3.28	3.18	3.04	3.25
K_2O	0.04	0.05	0.02	0.03	0.02	0.04
Total	102	102	102	100	100	98
Si	8.85	8.95	8.94	8.97	8.88	9.09
Al	6.95	6.87	6.87	6.70	6.81	6.57
Fe(ii)	0.00	0.01	0.01	0.01	0.01	0.00
Ca	3.33	3.20	3.22	3.42	3.47	3.36
Na	1.06	1.16	1.15	1.14	1.09	1.18
K	0.01	0.01	0.00	0.01	0.00	0.01
Ba	0.00	0.00	0.00	0.00	0.00	0.00
Total	20.21	20.20	20.20	20.25	20.26	20.22
No. of oxygens	32	32	32	32	32	32
End members						
An (%)	75.7	73.2	73.7	74.8	76.0	73.8
Ab	24.1	26.6	26.2	25.0	23.9	25.9
Or	0.2	0.3	0.1	0.2	0.1	0.2

Table 2. Amphibole compositional data of Temra metagabbros

Point	1	2	3	4	5
SiO_2 (wt%)	52.0	55.4	50.6	57.6	52.2
TiO_2	0.2	0.2	0.6	0.1	0.7
Al_2O_3	5.2	2.0	6.1	1.8	6.2
Cr_2O_3	0.2	0.1	0.6	0.2	0.2
FeO	9.4	7.8	9.6	8.1	9.7
MnO	0.3	0.2	0.2	0.3	0.2
MgO	17.2	19.6	16.6	19.3	16.6
CaO	13.1	14.3	13.9	14.0	13.1
Na_2O	0.50	0.15	0.59	0.18	0.52
K_2O	0.05	0.01	0.24	0.01	0.37
Total	98.3	99.7	99.0	101.6	99.7
No. of oxygens	8	8	8	8	8
Si	7.38	7.67	7.18	7.80	7.21
Al(iv)	0.62	0.33	0.82	0.20	0.79
Al(vi)	0.25	0.00	0.20	0.09	0.25
Fe(iii)	0.00	0.00	0.00	0.00	0.00
Ti	0.02	0.02	0.07	0.01	0.07
Cr	0.03	0.01	0.06	0.02	0.02
Fe(ii)	1.12	0.91	1.14	0.92	1.17
Mn	0.04	0.03	0.02	0.03	0.02
Mg	3.64	4.04	3.50	3.90	3.54
Ca	1.99	2.12	2.11	2.03	2.01
Na	0.14	0.04	0.16	0.05	0.14
K	0.01	0.00	0.04	0.00	0.07
Total	15.22	15.16	15.31	15.06	15.30
Si	7.38	7.67	7.18	7.80	7.21
Al(iv)	0.62	0.33	0.82	0.20	0.79
T	8	8	8	8	8
Al(vi)	0.25	0.00	0.20	0.09	0.25
Ti	0.02	0.02	0.07	0.01	0.07
Cr	0.03	0.01	0.06	0.02	0.02
Fe(iii)	0.00	0.00	0.00	0.00	0.00
Fe(ii)	1.12	0.91	1.14	0.92	1.17
Mn	0.04	0.03	0.02	0.03	0.02
Mg	3.64	4.04	3.50	3.90	3.54
C	5.09	5.00	4.99	4.98	5.07
C-5	0.09	0.00	0.00	0.00	0.07
Ca	1.99	2.12	2.11	2.03	2.01
Na	–0.08	–0.12	–0.11	–0.03	–0.08
B	2	2	2	2	2
Na	0.22	0.16	0.28	0.08	0.23
K	0.01	0.00	0.04	0.00	0.07
A	0.22	0.16	0.32	0.08	0.30
T/S	1.05	1.06	1.04	1.06	1.05
Fe(ii)	3.52	3.50	3.25	3.85	3.34
Fe(iii)	–2.34	–2.55	–2.06	–2.88	–2.12
$Fe^2/(Fe^2+Fe^3)$	3.00	3.66	2.73	3.94	2.74
$Fe^3/(Fe^3+Fe^2)$	–2.00	–2.66	–1.73	–2.94	–1.74
$Mg/(Mg+Fe^{2+})$	0.77	0.82	0.75	0.81	0.75
$Fe^3+/(Fe^3++(6)Al)$	0.00	0.00	0.00	0.00	0.00

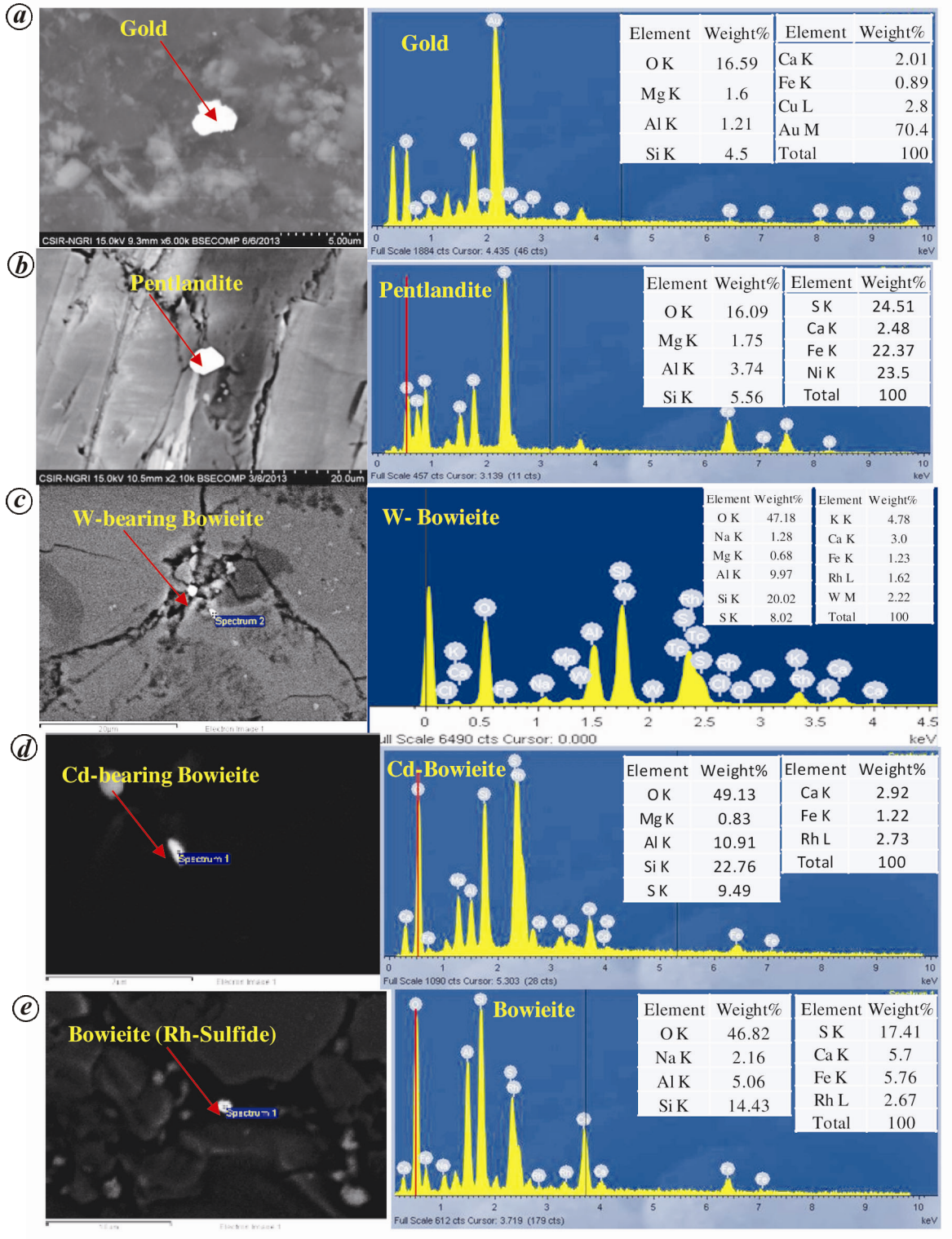

Figure 2. SEM-back scattered electron (BSE) images and EDS spectrum of different coexisting ore minerals from Temra area in the NW part of the Betul Belt.

oxide phases include abundant magnetite (FeO_T = 77.9–79.8%), minor ilmenite and rutile (TiO_2 = 97.9%). Sulphide mineralization is represented by two types such as the earlier Fe–Ni–Cu–Co sulphides occurring as fine disseminations, irregular blebs/grains located at the interstices between silicate or oxide minerals, and the later remobilized sulphides which exhibit stringer/veinlet morphology of Cu–Fe sulphides such as chalcopyrite and

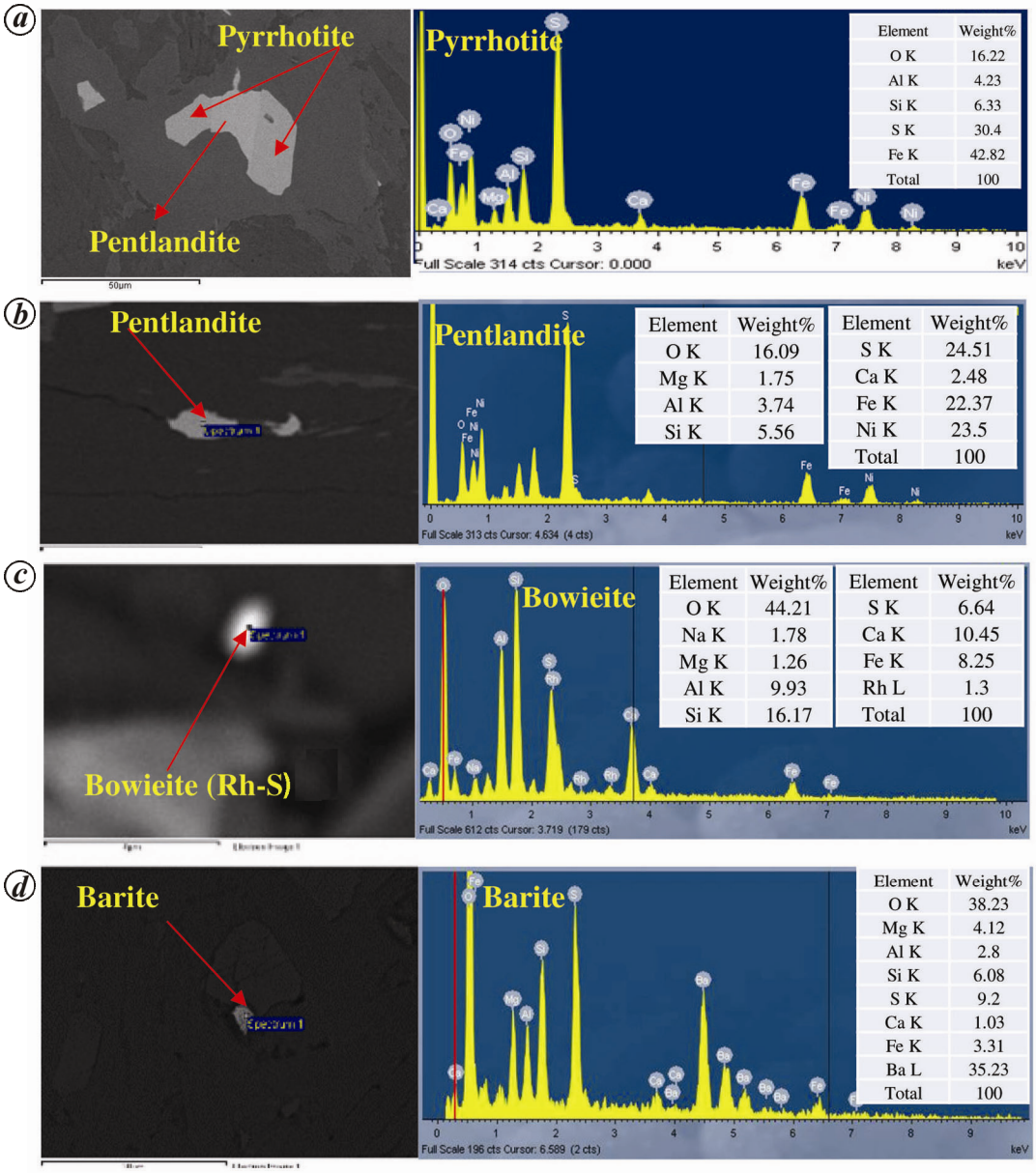

Figure 3. SEM-back scattered electron (BSE) image and EDS spectrum of different coexisting ore minerals from Sarni area in the south central part of the Betul Belt.

pyrite. The latter occur along the fracture planes and are related to post-magmatic enrichment processes.

The altered and sulphidic metagabbros of Sarni area are mainly composed of disseminations of pyrite, minor chalcopyrite, pyrrhotite and pentlandite as well as fine specks of bright palladium and rhodium bearing mineral phases. Pink, altered, quartz veins intruded the metagabbros. They show abundant visible sulphides. Detailed petrography/ore petrology and multi-element geochemistry of sulphide-bearing quartz veins form a subject matter of another study.

Characterization of sulphides and platinum group minerals (PGM) was done by Hitachi, S-3400N Scanning Electron Microscope (SEM) coupled with energy dispersive spectrometry (EDS) at CSIR-NGRI (Figures 2 and 3). Spot analysis of different ore minerals and back scattered electron (BSE) imaging were carried out to understand the compositions and variations of the different ore mineral phases.

Several ore minerals and mineral phases such as native gold and sulphides of Cu, Te, Ni, Pb, Rh, Rh–W, Zn as well cadmium-bearing phases are identified in the Temra gabbro anorthosite suite using the SEM–EDS. Some selected sulphides and PGMs which were identified by SEM in the Temra gabbroic suite are presented in Figure 2. These minerals include native gold, chalcopyrite, pentlandite, bowieite and Cd-bearing bowieite and zircon, which are identified for the first time from metagabbros

Table 3. Whole rock major, trace, rare earth and PGE compositional data of Temra and Sarni gabbroic suites

Sample	PDR-67	PDR-70	PDR-81	PDR-84	SRN-4	SRN-5	SRN-6	SRN-7
SiO_2 (%)	46.8	43.7	44.2	51.6	43.9	43.3	50.2	41.9
Al_2O_3	12.3	6.3	15.9	14.3	14.0	14.8	13.1	8.2
Fe_2O_3	11.8	9.7	5.8	9.9	12.8	12.9	6.3	11.5
MnO	0.2	0.2	0.1	0.1	0.1	0.2	0.1	0.2
MgO	16.2	23.9	25.5	13.0	16.2	16.4	13.3	23.5
CaO	10.2	8.6	0.6	7.5	8.7	8.2	11.7	6.4
Na_2O	1.1	0.1	1.2	1.0	1.6	1.3	1.8	0.3
K_2O	0.5	0.1	0.6	0.6	0.7	0.6	1.0	3.8
TiO_2	0.3	0.3	0.2	0.3	0.7	0.8	0.8	0.6
P_2O_5	0.01	0.07	0.03	0.02	0.17	0.15	0.12	0.21
LOI	1.2	5.9	6.0	2.4	1.8	1.5	1.6	3.6
Sum	100.6	98.9	100.0	100.9	100.7	100.1	100.0	100.1
Sc (ppm)	36.0	31.8	26.9	22.3	15.5	17.0	22.4	12.3
V	139.1	99.8	96.5	153.1	102.1	133.1	422.2	122.1
Cr	98.5	1188.3	336.3	908.6	70.6	103.5	255.9	825.9
Co	132.1	94.8	38.3	57.3	72.3	85.6	146.5	95.8
Ni	504.6	460.8	189.6	180.8	115.7	147.3	315.7	1016.7
Cu	1105.1	36.5	96.0	66.3	230.4	301.4	416.9	557.8
Zn	38.6	99.2	51.2	80.8	49.0	92.1	136.1	76.4
Ga	13.0	7.3	15.5	16.9	16.9	15.3	18.8	19.2
Rb	17.0	1.5	22.1	45.4	30.5	27.2	111.9	33.7
Sr	207.8	22.5	312.3	171.1	302.8	239.2	221.7	265.9
Y	7.1	11.5	5.8	6.9	12.5	12.4	32.3	10.7
Zr	12.5	33.8	13.9	9.6	12.5	15.0	40.8	10.7
Nb	0.3	3.8	0.5	0.3	2.3	2.5	9.4	1.0
Cs	8.4	0.4	23.7	4.2	12.0	10.4	9.0	8.3
Ba	40.8	44.4	110.0	131.3	148.1	139.2	434.5	229.8
La	4.0	6.0	4.9	6.6	8.9	8.7	17.1	7.1
Ce	7.6	8.5	8.9	12.2	16.1	16.1	35.2	13.6
Pr	1.1	1.7	1.1	1.6	2.2	2.2	5.3	1.8
Nd	4.8	7.5	4.9	6.6	9.8	9.7	24.8	8.4
Sm	1.2	1.8	1.0	1.5	2.3	2.1	5.6	2.1
Eu	0.5	0.5	0.5	0.6	1.0	1.0	1.0	0.9
Gd	1.2	1.7	1.0	1.6	2.2	2.2	6.0	2.1
Tb	0.2	0.3	0.2	0.2	0.4	0.4	1.0	0.4
Dy	1.0	1.6	0.8	1.2	1.7	1.8	4.5	2.0
Ho	0.2	0.3	0.2	0.3	0.4	0.4	0.9	0.4
Er	0.8	1.1	0.6	0.8	1.2	1.3	3.1	1.3
Tm	0.1	0.2	0.1	0.1	0.2	0.2	0.4	0.2
Yb	0.7	1.1	0.6	0.7	1.1	1.1	2.6	1.0
Lu	0.1	0.2	0.1	0.1	0.2	0.2	0.4	0.2
Hf	0.4	0.8	0.4	0.3	0.4	0.5	1.5	0.5
Ta	0.0	0.3	0.1	0.1	0.1	0.1	0.8	0.2
Pb	2.9	3.0	3.5	4.9	1.7	1.6	3.5	4.7
Th	0.6	1.4	0.7	0.6	1.2	1.3	2.6	0.6
U	0.1	0.4	0.3	0.1	0.1	0.1	0.4	0.1
Ru(ppb)	4	10	3	3	70	32	2	33
Rh	16	3	2	5	33	21	2	22
Pd	66	22	23	92	1117	790	12	303
Os	3	2	2	6	68	54	2	26
Ir	1	1	2	1	11	6	1	6
Pt	29	18	17	47	225	201	20	212
Au	64	20	29	93	56	58	18	46
∑PGE (ppb)	100.6	56	48	154	1524	1104	39	602
Eu/Eu*	1.33	1.38	0.82	1.69	1.24	1.40	1.34	0.51

of Temra area (PDR-69&82 samples) (Figure 2). PGMs occur along the interface of silicates and sulphides. SEM–EDS studies on Sarni metagabbros indicate the presence of pyrite, pyrrhotite, pentlandite and minor bowieite (Figure 3). In addition, rare occurrences of zircon and barite were also identified by SEM in the metagabbros of Sarni (Figure 3). As these minerals are tiny (5–50 μm), precious mineral inclusions are hosted in silicates as sulphides. The EDS spectra (Figures 2 and 3) show minor insignificant peaks of host mineral, mostly

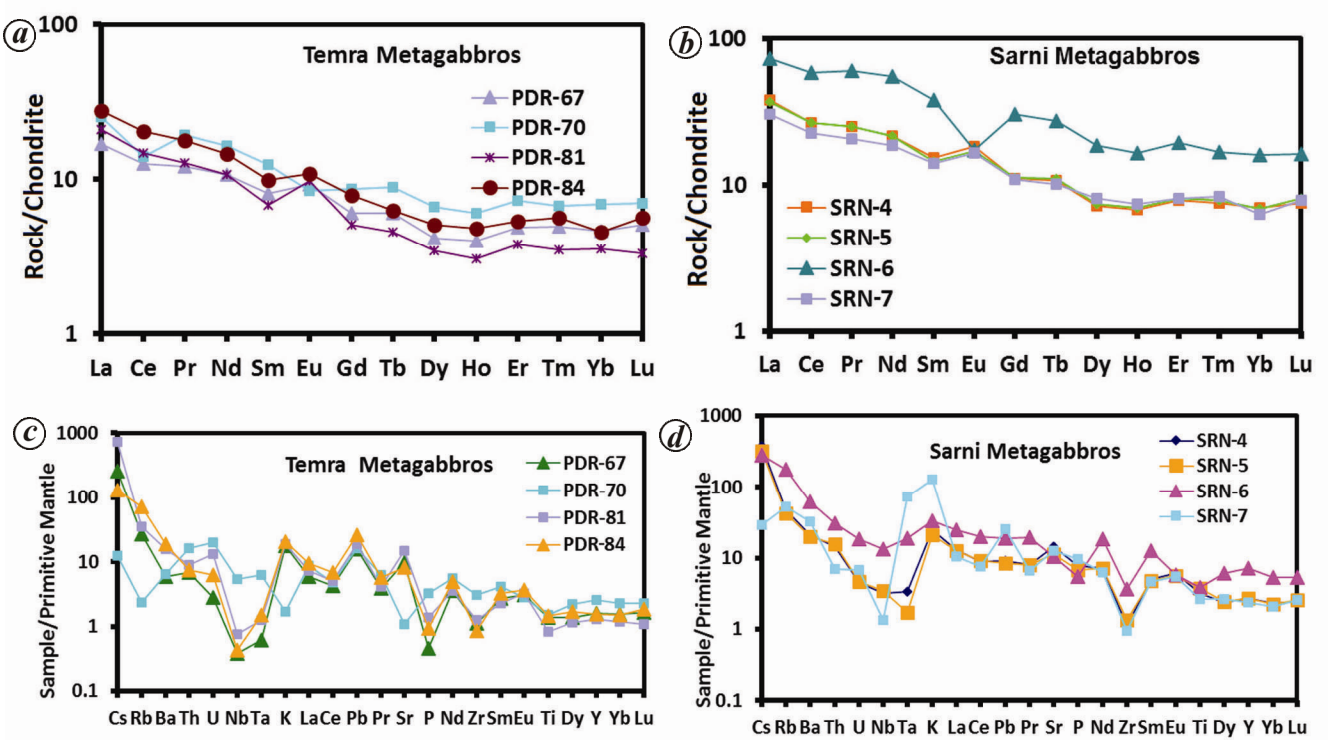

Figure 4. ***a***, Chondrite normalized REE patterns of the matagabbros of Temra area; ***b***, REE patterns of the metagabbros of Sarni area; ***c***, ***d***, Primitive mantle normalized trace element distribution patterns (Spidergram) of Temra and Sarni complexes in central India.

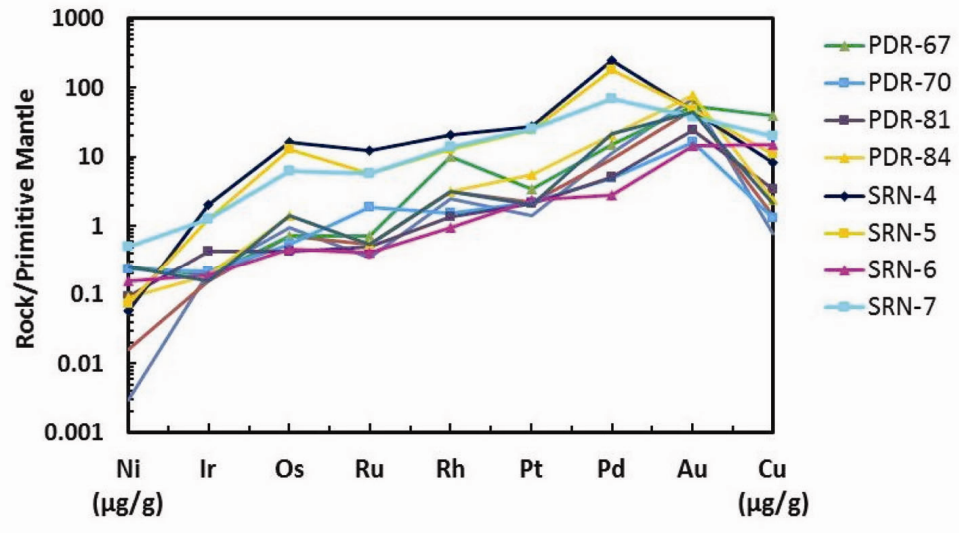

Figure 5. Primitive mantle normalized PGE distribution patterns of the Temra and Sarni metagabbros showing characteristic fractionated trends coupled with positive Rh and Pd anomalies.

silicates. Abundance of Os, Ru and Pd was insignificant and it has been suggested that Os, Pd and Ru are incorporated in pentlandite without forming individual mineral phases[12,13].

The mode of occurrence of native gold and RhS phases such as boewieite in the metagabbros of Temra within pentlandite and silicates coupled with their absence within fractures and planes of weakness in the host minerals, suggest their early crystallization and entrapment as orthomagmatic sulphide ores and silicates. This observation is also substantiated by intimate association of PGMs with Ni–Cu sulphides such as pyrrhotite and pentlandite bearing host metagabbro at Temra. Absence of characteristic replacement textures also suggests that there is no

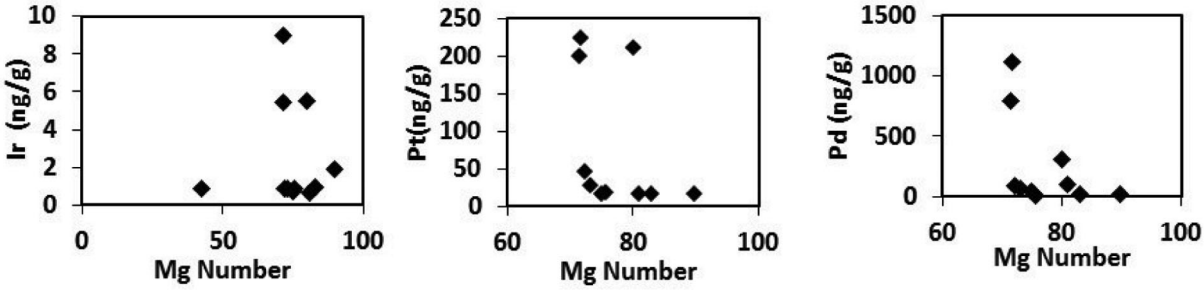

Figure 6. MgO relationship with Pt; Pd and Ir in Temra and Sarni Metagabbros.

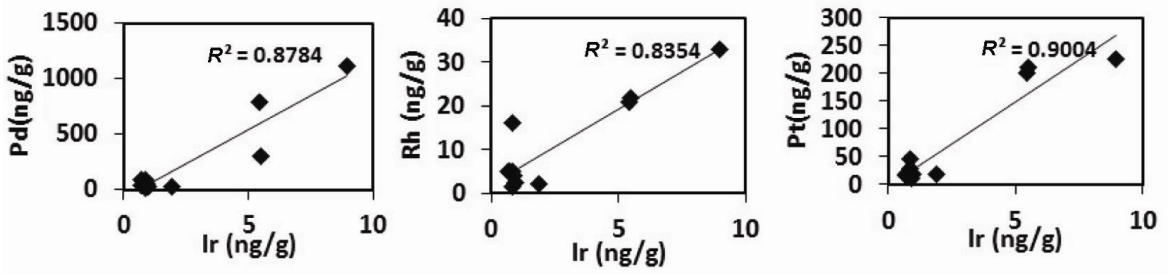

Figure 7. Binary plots showing the inter-element relationships of PGE.

interlinking of the native gold and PGE inclusions with the extensive penetrative later secondary hydrothermal activity, shearing and low to medium grade metamorphism which has affected the host metagabbro. The secondary hydrothermal fluids have interacted with the host metagabbro suites and as a result, simple mineralogy, i.e. pyrite–chalcopyrite and oxide ore minerals (magnetite) occur as large grains and minor stringers and veinlets throughout the host rock. Ni–Cu–Fe and PGE mineralization at Betul appears to have formed in two stages; one with primary magmatic Ni–Cu sulphide bearing PGE-poor sulphide ore and another as secondary epigenetic hydrothermal Cu–Fe-rich sulphide ores at Temra and Sarni suites of BC. The genesis of native gold, Ni–Cu sulphide hosted-PGE mineralization is related to primary magmatic differentiation and secondary remobilization/assimilation processes. Hydrothermal activity is evidenced by the presence of barite mineral phase (Figure 3) in the Sarni metagabbros. Hydrothermal alterations are also identified in the VMS-hosted horizons in the southeastern part of the Betul Belt[10], indicating the presence of shear zones at many places across the belt. The bulk rock major, trace, rare earth elements (REE) and PGE geochemical data are given in Table 3. Chondrite normalized REE patterns of the Temra metagabbros are characterized by slight light REE (LREE) enrichment, flat heavy REE (HREE) and positive Eu anomaly. Positive Eu anomaly (Eu/Eu* = 2.8) observed in gabbroic anorthosite (PDR-81 sample) is related to the presence of cumulus plagioclase and plagioclase accumulation in the melts of these rocks (Figure 4 *a*); whereas, the REE patterns of the Sarni metagabbros exhibit fractionated patterns with LREE enrichment, flat HREE and negative Eu anomaly (Eu/Eu* = 0.5), which indicate dominant plagioclase fractionation during partial melting (Figure 4 *b*). Sarni metagabbros have higher total REE (41.6–108.0 ppm) than the Temra gabbro-anorthosite suite (23.6–34.2 ppm). Primitive mantle normalized distribution patterns of metagabbros showing large ion lithophile elements (LILE) enrichment, positive Pb anomaly and negative Sr, Nb, Zr and Hf anomalies and flat HREE patterns suggesting that the parental magma of the complex was generated from a subduction modified, metasomatized, enriched mantle source and emplaced in a continental magmatic arc setting (Figure 4 *c* and *d*).

In addition, the total PGE concentrations in the metagabbros of Temra and Sarni complexes are determined by nickel sulphide fire assay method and inductive coupled plasma-mass spectrometer (ICP–MS) after following established procedures[14,15]. For PGE determination, repeated analysis of WMG-1 (Canadian Geological Survey) is used as CRM and WMS-1 is used as control standard. Detection limits of all the trace and RE elements were found to be in the range of 0.001 to 0.010 ng/g and the precision is <5% RSD. Detection limits for PGEs at 1 : 50 dilutions are Ru(101) = 0.016 ng/ml (16 ppt), Rh(103) = 0.01 ng/ml (10 ppt), Pd(105) = 0.01 ng/ml (10 ppt), Ir(193) = 0.005 ng/ml (05 ppt), Pt(195) = 0.04 ng/ml, (04 ppt), Au(197) = 0.010 ng/ml (10 ppt), precision =< 8% RSD[15]. Total PGE content in Temra metagabbros is low and varies from 77–119 ppb coupled with high concentrations of Cu (1613 ppm) and Ni

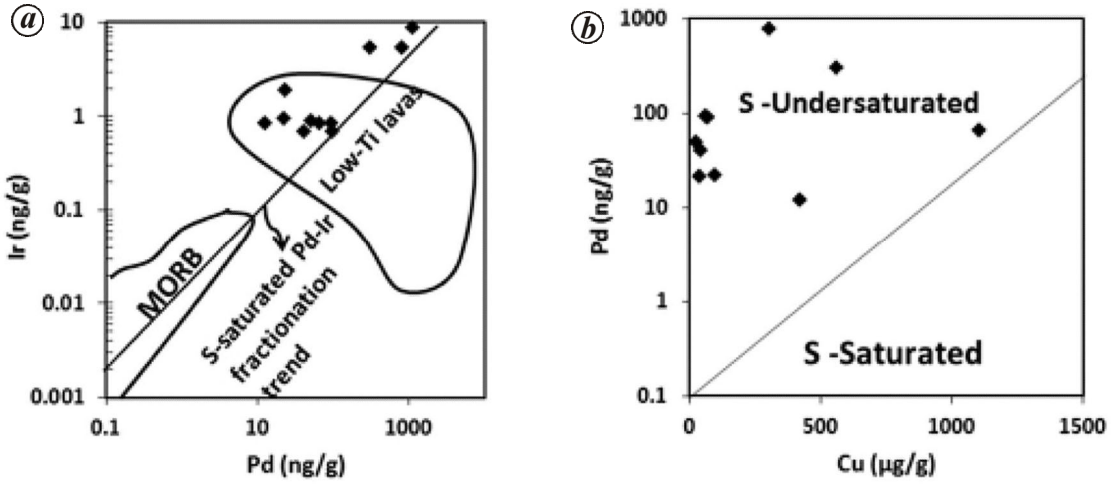

Figure 8. ***a***, Pd versus Ir binary plot for these metagabbro (Fields are after Hamlyn *et al.*[22]). ***b***, Plot of Cu versus Pd showing the sulphide undersaturation nature of magma (Fields are after Barnes *et al.*[16]).

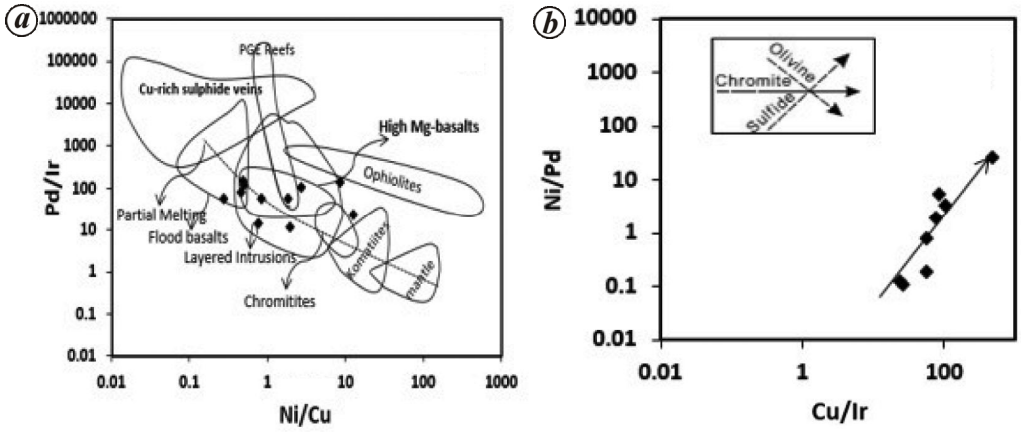

Figure 9. ***a***, Discrimination/plot showing Ni/Cu versus Pt/Ir in these matagabbros (Fields are after Barnes *et al.*[16]); ***b***, Binary plot of Ni/Pd versus Cu/Ir indicating that PGEs are fractionated by sulphides only (Fields are after Hoatson and Keys[23]).

(1946 ppm) (PDR-67 sample), indicating dominant presence of Ni–Cu sulphides such as pyrrhotite, chalcopyrite and pentlandite. In contrast, the Sarni metagabbros have anomalous ∑PGE values (∑PGE = 1104–1524 ppb) in which Pd is always greater than Pt in its abundance and PPGE > IPGE. It was observed that the PGE content increases in the presence of sulphides in the host metagabbros from Sarni.

PGE patterns of the anomalous Temra and Sarni gabbro-anorthosite suite exhibit an upward fractionated trend with strong positive Rh and Pd anomalies indicating the presence of RhS minerals (Bowieite) and Pd (Figure 5). The binary plots of Mg number versus Pt, Pd and Ir in the Temra and Sarni samples indicate that early fractionated mafic mineral phases had no control on the obtained PGE concentrations (Figure 6). Binary inter-element PGE plots such as Pd versus Ir and Pt versus Ir show sympathetic trends with a high correlation coefficient ($R^2 = 0.9$). These inter-element relationships of PGE indicate their fractionation by a similar sulphide phase (Figure 7). In addition to this, the binary plot of Pd versus Ir suggests that parental magmas are primitive in nature having high-Mg, low-Ti characteristics representing boninitic/picritic nature of magmas (Figure 8 *a*). The Cu versus Pd plot also shows sulphur undersaturation of magmas (Figure 8 *b*). The Ni/Cu versus Pd/Ir ratio plot indicates the involvement of partial melting of mantle and discriminates these samples as high Mg-basalts[16] (Figure 9 *a*). Finally, the relationships between Ni/Pd versus Cu/Ir show that these samples follow a clear sulphide fractionation trend and reveal that the PGEs are fractionated by sulphides (Figure 9 *b*). The trace, REE and PGE geochemistry of Temra and Sarni gabbro-anorthosites are comparable to those of the fractionated mafic intrusions characteristic of many Proterozoic intrusive ultramafic–mafic complexes of the world. The Ni–Cu–PGE

mineralization in Betul complex show similarities to the Pd–PGE Group of the Geordie Lake intrusion, Ontario which contains Pd, Pt, Rh and Au[17] as well as Voisey's Bay Ni–Cu–Co deposit, Labrador, Canada[12] and PGE-poor Cu-rich magmatic sulphides from Lalatongke deposit, Xinjiang, NW China[13]. This study serves as an example of late stage hydrothermal modification of early formed orthomagmatic sulphide ores. Thus, the PGE mineralization in both Temra and Sarni metagabbros is governed by orthomagmatic sulphides, whereas the incorporation of native gold and Cu–Fe sulphides is the result of late stage hydrothermal activity. This new find of native gold and platinoids in association with silicate phases, Ni–Cu–Fe and base metal sulphides, etc., opens up a new region for Ni–Cu–PGE exploration in the several exposed and less-studied ultramafic–mafic intrusives emplaced in the BFB within the CITZ, central India. Further studies on PGE metallogeny of these important Betul ultramafic–mafic magmatic rocks would improve our present day understanding on the mantle processes such as mantle melting, sulphur saturation (R-factor) and later crustal assimilation processes involved in the enrichment of PGE ores during the Proterozoic.

1. Condie, K. C., *Proterozoic Crustal Evolution*, Elsevier, Amsterdam, 1992.
2. Roy, A. and Prasad, H. M., Tectonothermal events in Central Indian Tectonic Zone (CITZ) and its implication in Rhodinian crustal assembly. *J. Asian Earth. Sci*., 2003, **22**, 115–129.
3. Bhowmik, S. K., Pal, T., Roy, A. and Pant, N. C., Evidence for Pre-Grenvillian high pressure granulite metamorphism from the northern margin of the Sausar mobile Belt in central India. *J. Geol. Soc. India*, 1999, **53**, 385–399.
4. Roy, A. *et al.*, Rb–Sr and Sm–Nd dating of different metamorphic events from the Sausar mobile belt, Central India: implications for proterozoic crustal evolution. *J. Asian Earth Sci*., 2006, **26**, 61–76.
5. Roy, S., Sedimentary manganese metallogenesis in response to the evolution of the Earth system. *Earth Sci. Rev*., 2006, **77**, 273–305.
6. Bhowmik, S. K., Sarbadhikari, A. B., Spiering, B. and Raith, M., Mesoprotrozoic reworking of palaeoproterozoic ultrahigh-temperature granulites in the Central Indian Tectonic zone and its implications. *J. Petrol*., 2005, **46**, 1085–1119.
7. Mahakud, S. P., Raut, Hansda, C., Ramteke, F. P., Chakraborty, U., Praveen, M. N. and Sisodia, D. S., Sulphide mineralization in the central part of Betul belt around Ghisi–Mauriya–Koparapani area, Betul district, Madhya Pradesh. *Geol. Surv. India Spec. Publ.*, 2001, **64**, 377–385.
8. Ramachandra, H. M., A review of terrain evolution in the precambrian Dharwar and Bastar Craton. *Geol. Soc. India, Spec. Publ.*, 2004, **84**, 1–21.
9. Praveen, M. N., Biswajit Ghosh, Shrivastava, H. S., Dora, M. L. and Gaikawad, L. D., Sulphide mineralisation in Betul Belt: classification and characteristics. *J. Geol. Soc. India*, 2007, **69**, 85–91.
10. Golani, P. R., Dora, M. L. and Bandopdhyay, B. K., Base metal mineralization associated with hydrothermal alteration in Felsic volcanic rocks in Proteozoic Betul belt at Bhuyari, Chhindwara District, Madhya Pradesh. *J. Geol. Soc. India*, 2006, **68**, 797–808.
11. Ghosh, B. and Praveen, M. N., Indicator Minerals as guides to base metal sulphide mineralization in Betul Belt, Central India. *J. Earth Sys. Sci.*, 2008, **117**(4), 521–536.
12. Naldrett, A. J., Keats, H., Sparkes, K. and Moore, R., Geology of the Voisey's Bay Ni–Cu–Co deposit, Labrador. *Can. Explor. Min. Geol*., 1996, **5**, 169–179.
13. Gao, J. F., Zhou, M. F., Ligiitfoot, P. C., Wang, C. Y. and Gao, L. O., Origin of PGE-poor and Cu-rich magmatic sulfides from the Kalatongke Deposit, @2012 Society of Economic Geologists, Inc. *Econ. Geol.*, 2012, **107**, 481–506.
14. Balaram, V., Recent advances in the determination of PGE in exploration studies – a review. *J. Geol. Soc.*, 2008, **72**, 661–677.
15. Balaram, V., Mathur, R., Banakar, V. K., James, R. Hein, Rao, C. R. M., Gnaneswara Rao, T. and Dasaram, B., Determination of the platinum-group elements and gold in manganese nodule reference samples by nickel sulphide fire-assay and Te-coprecipitation with ICP-MS. *Indian J. Mar. Sci*., 2006, **35**(1), 7–16.
16. Barnes, S.-J., Boyd, R., Korneliussen, A., Nilsson, L.-P., Often, M., Pedersen, R. B. and Robins, B., The use of mantle normalization and metal ratios in discriminating between the effects of partial melting, crustal fractionation and sulphide segregation on platinum group elements, gold, nickel and copper: Examples from Norway, 1988. In Geoplatinum-87 (eds Prichard, H. M. *et al.*), Elsevier, London, 1988, pp. 113–143.
17. Mulja, T. and Mitchell, R. H., The Geordie Lake Intrusion, cold well complex, Ontario: a palladium and tellurium-rich disseminated sulphide occurrence derived from evolved tholeiitic magma. *Econ. Geol*., 1991, **86**, 1050–1069.
18. Deb, M., Precambrain geodynamics and metallogeny of the Indian shield. *Ore Geol. Rev*., 2014, **57**, 1–28.
19. Acharya, S. K., A palte tectonic model for Proterozoic crustal evolution of central Indian tectonic zone. *Gondwana Res*., 2003, **7**, 9–31.
20. Meert, J. G. *et al.*, Precambrian crustal evolution of Peninsular India: a 3.0 billion year odyssey. *J. Asian Earth Sci*., 2010, **39**, 483–515.
21. Roy, A., Chore, S. A., Viswakarma, L. L. and Chakraborthy, K., Geology and perochemistry of Padhar mafic–ultramafic complexes from Betul Belt: a study on arc type magmatism in central Indian Tectonic zone. *Geol. Surv. India Spec. Publ*., 2004, **84**, 297–318.
22. Hamlyn, P. R., Keays, R. R., Cameron, W. E., Crawford, A. J. and Waldron, H. M., Precious metals in magnesian low-Ti lavas: implications for metallogenesis and sulfur saturation in primary magmas. *Geochim. Cosmochim. Acta*, 1985, **49**, 1797–1911.
23. Hoatson, D. and Keays, R., Formation of platiniferous sulfide horizons by crystal fractionation and magma mixing in the Munni Munni layered intrusion, West Pilbara Block, Western Australia. *Econ. Geol.*, 1989, **84**, 1775–1804.

ACKNOWLEDGEMENTS. We thank Dr Y. J. Bhaskar Rao, Acting Director, National Geophysical Research Institute (CSIR-NGRI) for his kind permission to publish this paper. We also thank Drs E. V. S. S. K. Babu and A. Keshav Krishna who have provided the EPMA and XRF analyses at CSIR-NGRI Geochemistry Laboratories. We are thankful to Dr S. N. Charan for critical review of the manuscript. We are also thankful to the anonymous reviewers for their useful suggestions and editorial handling which have improved the paper significantly. This work has been carried out under the on-going CSIR-NGRI 12th FYP SHORE Project WP 4.2.

Received 28 June 2014; revised accepted 27 October 2014